Journal of Alloys and Compounds 658 (2016) 440–452

Contents lists available at ScienceDirect

Journal of Alloys and Compounds

journal homepage: http://www.elsevier.com/locate/jalcom

Preparation and characterization of NiCrAlY/nano-YSZ/PCL composite coatings obtained by combination of atmospheric plasma spraying and dip coating on Mg–Ca alloy

H.R. Bakhsheshi-Rad [a, *], E. Hamzah [a], A.F. Ismail [b], M. Daroonparvar [a], M.A.M. Yajid [a], M. Medraj [c, d]

[a] Department of Materials, Manufacturing and Industrial Engineering, Faculty of Mechanical Engineering, Universiti, Teknologi Malaysia, 81310 Johor Bahru, Johor, Malaysia
[b] Advanced Membrane Technology Research Center (AMTEC), Universiti Teknologi Malaysia, 81310 Skudai, Johor Bahru, Johor, Malaysia
[c] Department of Mechanical Engineering, Concordia University, 1455 De Maisonneuve Blvd.West, Montreal, QC H3G 1M8, Canada
[d] Mechanical and Materials Engineering, Masdar Institute, Abu Dhabi, PO Box 54224, United Arab Emirates

ARTICLE INFO

Article history:
Received 9 July 2015
Received in revised form
15 September 2015
Accepted 20 October 2015
Available online 23 October 2015

Keywords:
Mg alloy
Biodegradable
Triplex coating
Corrosion resistance
Mechanical properties

ABSTRACT

A triple-layer NiCrAlY/nano-yttria stabilized zirconia (nano-YSZ)/polycaprolactone (PCL) coating was deposited on Mg–Ca alloy by novel combination of atmospheric plasma spraying (APS) and dip coating methods, aiming at further enhancement of the corrosion and mechanical properties of the Mg alloy. The compressive strength of the triple-layer plasma/polymer coating is higher than that of the plasma coated and uncoated samples after immersion in 3.5 wt% NaCL solution. However, both single and dual-layer plasma coatings demonstrated better bonding strength than the triple-layer plasma/polymer coating. The corrosion resistance of Mg alloy was significantly improved by triple-layer NiCrAlY/nano-YSZ/PCL coating this was inferred from the lower corrosion current; 0.14 μA/cm^2 versus 285.3 μA/cm^2 for the uncoated Mg alloy, the higher corrosion potential; −1252.8 versus −1631.4 mV$_{SCE}$, and the significantly lower corrosion rate; 0.003 versus 6.51 mm/yr. A corrosion mechanism for the single-, double- and triple-layer coated Mg alloy was proposed. PCL coating provides significant protection for the Mg alloy by sealing the porous nano-YSZ plasma coating.

1. Introduction

Magnesium alloys have great potential for automotive, aerospace, medical orthopaedic, and other industries due to their low density, high specific strength, machinability, and damping characteristic [1–3]. Various binary Mg alloys based on Ca, Zn, Y additions were applied for improving corrosion properties of pure Mg [4]. Addition of Ca lower than its solid solubility limit (1.34 wt.%) to Mg decreases the corrosion rate of pure Mg. Likewise, the addition of 1.2 wt.% Ca tend to improve the compressive strength and bending strength of pure Mg due to decrease the grain size and solution strengthening effects and second phase strengthening [5]. However, intrinsic deficiencies such as poor corrosion resistance inhibit the widespread use of Mg alloys in many applications [6,7]. Thus, it is essential to enhance the corrosion resistance of Mg to broaden their industrial applications [8]. Hence, surface modification was employed as an effective strategy to protect Mg alloys from corrosion attack [7,9–11]. Atmospheric plasma spraying (APS) is an effective coating method for improving the surface properties of different alloys [12]. This is because APS is a fast and an environment-friendly process that has the ability to deposit high-quality ceramic coating [13]. APS is also applied for fabrication of nanostructured ceramic coatings (such as YSZ) having good mechanical and corrosion properties [13–16]. The structure of APS coating consists of a large amount of micro-porosity and micro-cracks which assist in releasing residual stresses, while at the same time produce a mechanical interlocking effect in the outer layer that can considerably enhance the adhesion of polymeric overlayer [1]. Commonly used thermal barrier coating (TBS) materials such as ZrO_2 and 8YSZ are usually employed as ceramic top coat materials on a metallic bond-coat such as MCrAlY or NiCrAlY

* Corresponding author.
E-mail addresses: bhamidreza2@live.utm.my, rezabakhsheshi@gmail.com (H.R. Bakhsheshi-Rad).

http://dx.doi.org/10.1016/j.jallcom.2015.10.196
0925-8388/

[17]. The use of a bond-coat decreases thermal expansion coefficient mismatch between the ceramic top coat and the substrate, increases the adhesion of the top coat to the Mg substrate and prevents debonding [12,18]. However, the porosities of plasma coating also can absorb more aggressive medium leading to more infiltration of corrosive species to the substrate [1]. The existence of these porosities is unavoidable in the plasma spray coatings resulting in inferior chemical barrier performance [17,19]. Therefore, several researchers [2,8,19] attempted to seal the micro-pores to enhance the corrosion resistance of the substrate. Polymeric coating is an effective approach for sealing the porosity of plasma layers to avoid early failure. Among the polymer coating, polycaprolactone (PCL; $-[(CH_2)_5COO]_n-$) as a semi crystalline linear hydrophobic polymer can be considered as one of the promising candidates because of its good mechanical properties such as the high ductility of 80% elongation at the break point [20,21]. In addition, PCL is hydrophobic, which is desirable for a coating as top layer on plasma porous layer to fill its porosity and to further improve the corrosion resistance of the substrate [21,22]. In view of this, Mohedano et al. [19] showed that the corrosion properties of the plasma coatings enhanced after sealing plasma layer. Similarly, Gnedenkov et al. [11] reported that protective performance of the polymer-containing composite coating was 300-fold higher compared to the initial plasma coating. However, studies on the surface modification of Mg alloys by NiCrAlY/nano-YSZ/PCL triple-layer coating aimed at further improving the corrosion and mechanical properties of Mg-based alloys could not be found in the literature. Thus, in the present study, combinations of APS and dip coatings were conducted to provide a triple-layer coating system which integrates the advantages from both methods. After the NiCrAlY and nano-YSZ coating on Mg–Ca alloy as first and second layer respectively, a PCL was employed on top of plasma layers to seal the pores and to provide further protection for the Mg–Ca substrate. The microstructure, mechanical properties and corrosion behaviour of uncoated Mg–Ca alloy, NiCrAlY, NiCrAlY/nano-YSZ and NiCrAlY/nano-YSZ/PCL coatings were evaluated and compared.

2. Experimental details

2.1. Sample preparation

Magnesium alloys were prepared by melting 99.9% pure magnesium ingots, and Mg–32 wt.% Ca. The melts, with a constant concentration of Ca (2.5 wt.%), were then cast in a 300 °C preheated stainless steel mould to produce an ingot. Several Mg–1.2 wt.% Ca rectangular specimens with dimensions of 15 mm × 10 mm × 10 mm, and cylindrical specimens with a diameter of 10 mm and thickness of 10 mm were cut from the ingot. The samples were mechanically wet ground with 320–2000 SiC grit papers until all visible scratches were removed. The overall composition was measured using ICP-AES as 0.047% Si, 0.003% Cu, 2.511% Ca, 0.021% Al, 0.012% Fe, 0.004% Ni and Mg balance.

2.2. Deposition of NiCrAlY/nano-YSZ/PCL coatings

A commercial NiCrAlY (Ni22Cr10Al1Y; AMDRY 962) powder with 40–65 μm particle size and agglomerated nanostructured YSZ powder (ZrO_2-8 wt.%Y_2O_3; Nanox Powder S4007, Inframat USA) were used to deposit the underlayer and overlayer, respectively. It should be mentioned that single nano-particles are very difficult to spray due to their low mass and inertia. To address this issue reconstitution of the nanoparticles into micrometre sized granules is vital [12].

As can be observed in Fig. 1, both feedstock powders particles have spherical morphology which is suitable for plasma spray. The high magnification inset of the nanostructured YSZ powder further confirms that the agglomerates consist of individual nano-particles of YSZ. For better adhesion of the coating the surface of magnesium alloy was grit blasted with alumina particles and subsequently the specimens were rinsed with acetone. An atmospheric plasma spray (METCO, type 3 MB) was used for the deposition of NiCrAlY and nanostructured YSZ layers. The spraying parameters are summarized in Table 1. 2.5 wt.% PCL pellets (M_w = 80,000 g/mol, Sigma–Aldrich, UK) were dissolved in dichloromethane (DCM; CH_2Cl_2, Sigma–Aldrich, UK) by stirring for 6 h at room temperature. The double-layer coatings were dipped in the PCL solution for 30 s and withdrawn at a constant speed to form a uniform coating and then dried at room temperature.

2.3. Mechanical properties

For compression test, standard samples were prepared according to ASTM E9 and immersed in 3.5wt.% NaCl for 10 days. To remove the surface corrosion product, samples were cleaned in a boiling solution of chromium trioxide (CrO_3). The specimens were then dried in warm air. Compression tests were performed using an Instron-5569 universal testing machine at a displacement rate of 0.5 mm/min, at ambient temperature. For each testing condition, two specimens were examined. The bonding strength of the NiCrAlY, NiCrAlY/nano-YSZ and NiCrAlY/nano-YSZ/PCL coated specimens was measured according to ASTM F1044 standard using a universal testing machine, Instron-5569. Cylindrical specimens with a diameter of 30 mm and a thickness of 10 mm were prepared. The cross-head displacement rate was 1 mm/min with a 10 kN load cell. Three coated specimens were tested and the average value was reported. The average of five microhardness readings acquired from the cross-section of the plasma coatings using a Vickers hardness tester (Shimadzu) using a 500 g for 15s was taken.

2.4. Corrosion testing and analysis

Rectangular specimens with a surface area of 1 cm^2 were mounted in epoxy resin for electrochemical testing. Electrochemical tests were conducted in an open-air glass cell containing 350 ml of 3.5 wt.% NaCl, using a PARSTAT 2263 potentiostat/galvanostat (Princeton Applied Research). A three-electrode cell was used for potentiodynamic polarization testing. The reference electrode was a saturated calomel electrode (SCE), the counter electrode was a graphite rod, and the specimen was the working electrode. The samples were immersed in the NaCl solution for 1 h prior to the PDP test to establish the open-circuit potential. All experiments were carried out in the range between −250 mV in the cathodic direction and +500 mV in the anodic direction relative to the open circuit potential at a constant scan rate of 0.5 mV/s. The electrochemical impedance spectra (EIS) were measured at open circuit potential, with a 10 mV potential perturbation over a frequency range of 0.01 Hz–100 kHz at different immersion times in 3.5% NaCl solution, using a VersaSTAT 3 machine. Each electrochemical test was repeated 3 times to confirm reproducibility of the results. The corrosion current density (i_{corr}), corrosion potential (E_{corr}), cathodic Tafel slopes (β_c), anodic Tafel slopes (β_a), polarization resistance (R_P), and corrosion rate (P_i) were determined. The values of i_{corr}, E_{corr}, β_c, β_a, and a corresponding corrosion rate (P_i) for uncoated and coated samples were extracted from the polarisation curves. The polarisation resistance (R_P) was calculated according to the following equation [23]:

$$R_P = \frac{\beta_a \beta_c}{2.3(\beta_a + \beta_c) i_{corr}} \quad (1)$$

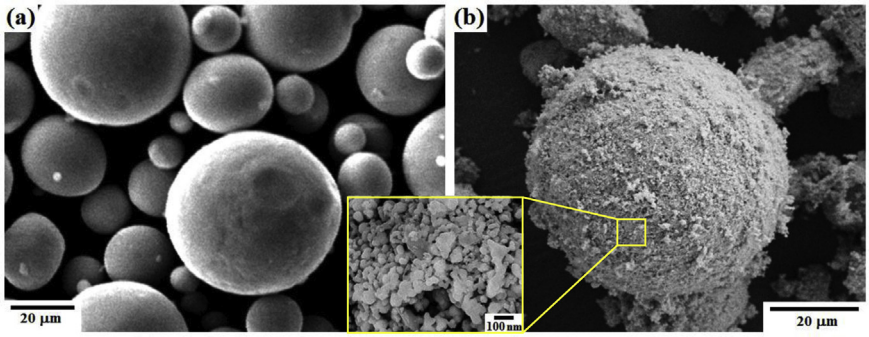

Fig. 1. Surface morphology of (a) NiCrAlY powders and (b) agglomerated nano-YSZ powders.

Table 1
Air plasma spraying parameters.

Parameters	NiCrAlY	Nano-YSZ
Current (A)	400	400
Voltage (V)	50	50
Primary gas, Ar (l/min)	60	60
Secondary gas, H_2(l/min)	8	8
Powder feed rate (g/min)	15	20
Spray distance (cm)	12	10

The corrosion rate of the samples, obtained from the corrosion current density, was calculated according to [24]:

$$P_i = 22.85\, i_{corr} \quad (2)$$

Immersion test was carried out according to ASTM G1-03. Specimens with a diameter of 10 mm and 10 mm thickness were immersed in a beaker containing 200 ml of 3.5 wt.% NaCl solution for 10 days. The immersion tests were repeated at least once to verify the reproducibility of the results.

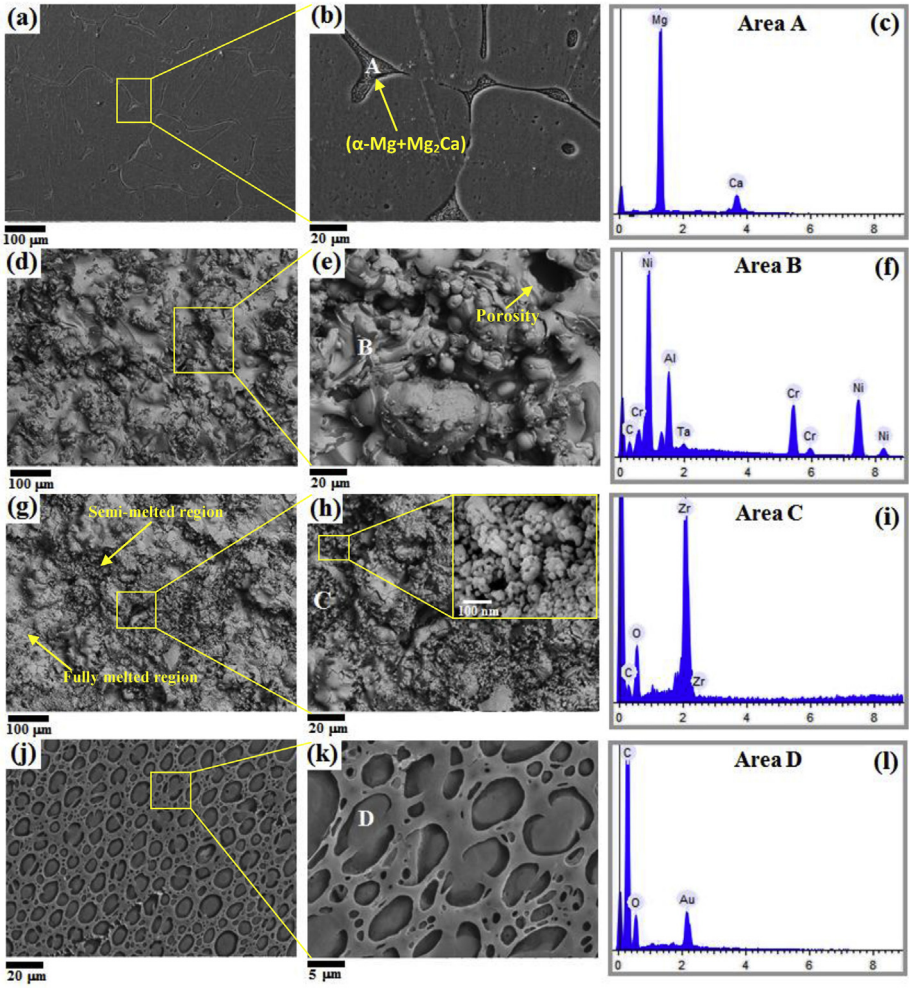

Fig. 2. Surface morphology of (a,b) uncoated Mg alloy, (d,e) single-layer NiCrAlY coating, (g,h) dual-layer NiCrAlY/nano-YSZ coating and (j,k) triple-layer NiCrAlY/nano-YSZ/PCL coated Mg alloy and EDS analysis of (c) area A, (f) area B, (i) area C and (l) area D.

2.5. Microstructural characterization

Microstructures were analysed with scanning electron microscopy (JEOL JSM-6380LA equipped with EDS system, JEOL Inc., Tokyo, Japan) and transmission electron microscopy (HT7700 Hitachi). Phase identification was carried out using an X-ray diffractometer (Siemens-D5000), using Cu-Kα radiation ($\lambda = 1.5405$ Å) generated at 35 kV and 25 mA, over the 2θ range of 10–90° with increment steps of 0.04.

3. Results and discussion

3.1. Characterization of the coating

Fig. 2 shows SEM images of uncoated, plasma sprayed and polymer/plasma coated Mg samples. Binary Mg–2.5Ca alloy consists of Mg_2Ca intermetallic compound in addition to α-Mg matrix which is consistent with the Mg–Ca phase diagram [25]. Secondary phases appear along the grain boundary (Fig. 2a,b) as eutectic phases (α-Mg + Mg_2Ca). The presence of secondary phases can significantly affect the corrosion behaviour of the Mg alloy due to the formation of micro-galvanic cells between the matrix and secondary phases [26–28]. The corresponding EDS analysis, in the denoted area, further confirmed that the grain boundaries were enriched with calcium which indicated the formation of Mg_2Ca (Fig. 2c). The single-layer NiCrAlY and dual-layer NiCrAlY/nano-YSZ coating composed of pores, voids and micro cracks due to the residual stresses during the deposition process (Fig. 2d,e) [29]. However the amount of pores, and micro cracks is significantly lower in the dual-layer coating compared to the single-layer counterpart (Fig. 2g,h). Semi-molten particles (SM) and molten particles (M) are also observed. It is reported that semi-molten particles contain porous structure, while molten parts bonded with each other to form a dense structure [30,31]. The dual-layer coating also showed nano-zone part which is composed of nano-sized particles that can be retained from the non-molten part of powder [13]. Large number of nano-pores with various sizes can be observed in this zone which has substantial effect on the corrosion behaviour of the plasma spray coated alloy. EDS analysis shows high amount of Ni, Al and Cr accompanied with low content of Y, indicating the formation of NiCrAlY coating (Fig. 2f). However, nano-structure YSZ coating is composed of Zr, O and trace amount of Y (Fig. 2i). The PCL coating over NiCrAlY/nano-YSZ layers (Fig. 2j,k) shows porous structure with relatively uniform distribution. The PCL as a top layer seals the micro-pores and voids in the plasma coating (Fig. 2j,k). The pores size is strongly dependent on the concentration of the PCL, where a high PCL concentration leads to formation of smaller pores due to the presence of less polymer-poor phase. The presence of pores in the PCL layer was mainly due to phase separation process, which is a result of solvent evaporation from the polymer solution. The pores formed because the polymer solution became thermodynamically unstable during solvent evaporation [21,32]. Phase separation resulted in the formation of either a polymer-rich or polymer-poor phases [33] where the polymer-rich phase would be solidified, whereas the polymer-poor phase led to pore formation [21,33]. This kind of distribution provides adhesion between the polymer coating and plasma coating. The pores size is strongly dependent on the concentration of the PCL, where a high PCL concentration leads to formation of smaller pores due to the presence of less polymer-poor phase [21]. EDS analysis (Fig. 2*l*) illustrates the presence of C and O in this sample, indicating the formation of PCL film.

Elemental mapping of the uncoated Mg–Ca alloy (Fig. 3a) confirmed that the grain boundaries were enriched with Ca, suggesting the presence of Mg_2Ca in the eutectic structure. The single-layer coating predominantly consisted of Ni, Cr, Al, O and trace amount of Y whilst the dual-layer coating is composed of Zr, O and Y which were uniformly distributed on the substrate (Fig. 3b,c).

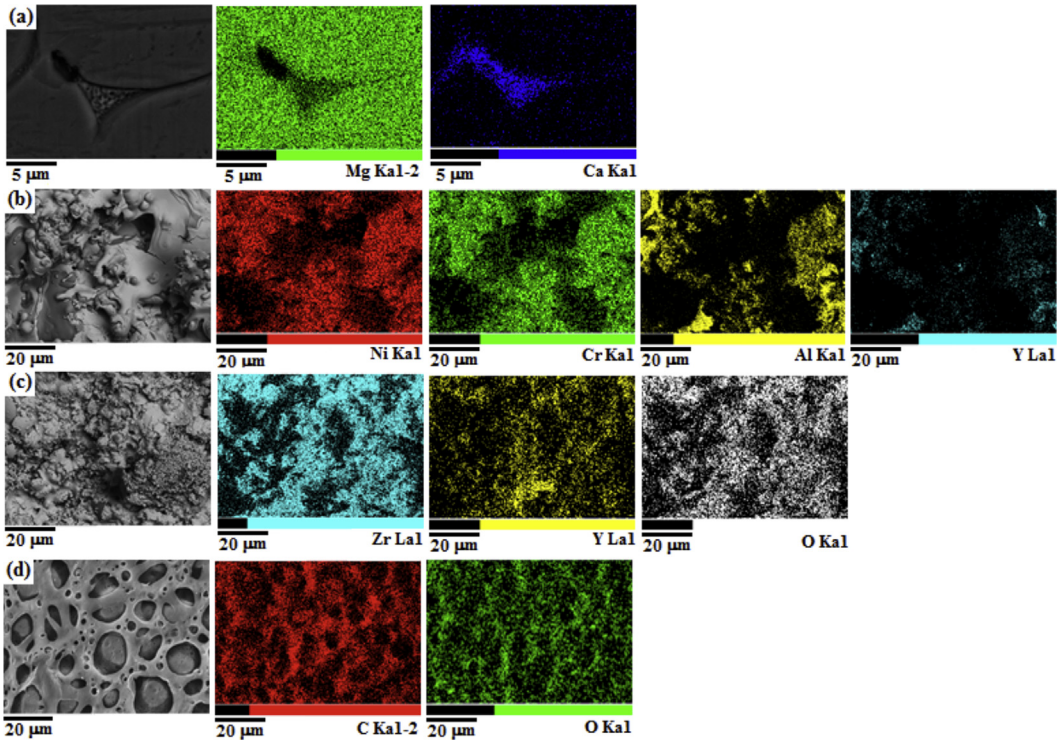

Fig. 3. Scanning electron micrographs and elemental mapping of (a) uncoated Mg alloy, (b) NiCrAlY coating, (c) NiCrAlY/nano-YSZ coating and (d) NiCrAlY/nano-YSZ/PCL coated Mg alloy.

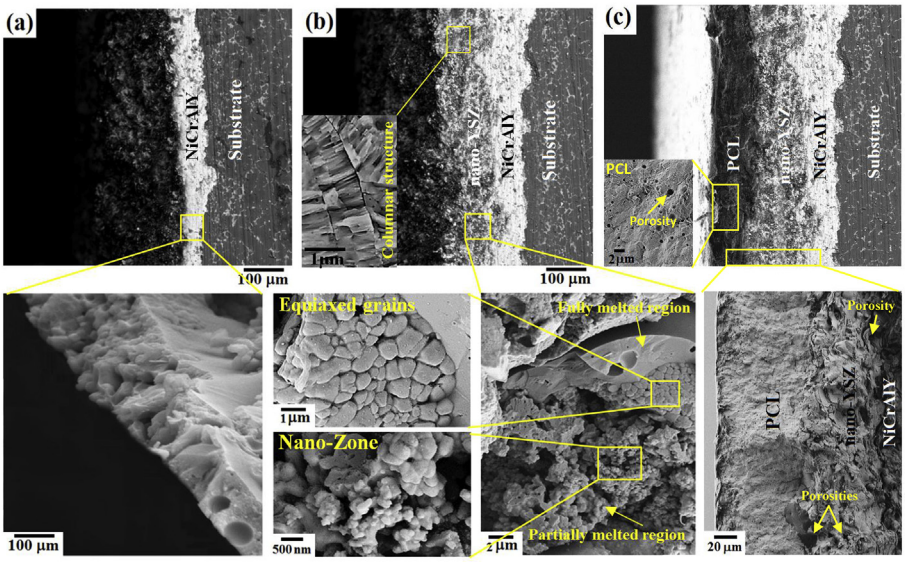

Fig. 4. Cross sectional SEM micrographs of (a) single-layer NiCrAlY, and (b) dual-layer NiCrAlY/nano-YSZ and (c) triple-layer NiCrAlY/nano-YSZ/PCL coated Mg alloy.

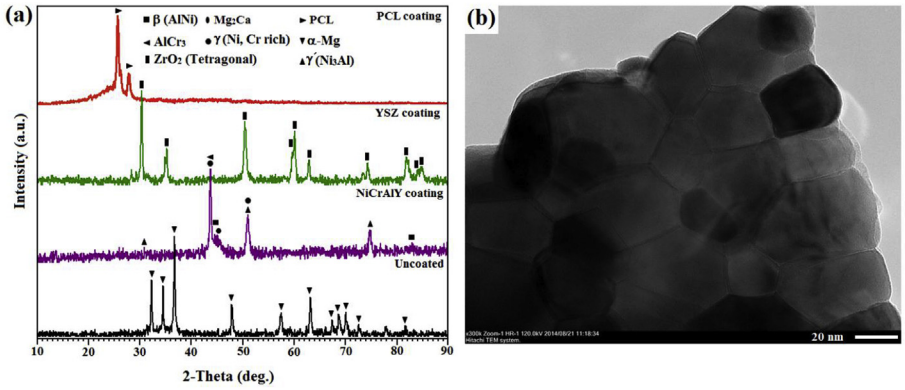

Fig. 5. (a) X-ray diffraction patterns of uncoated, NiCrAlY coating, nano-YSZ coating and PCL coated Mg alloy and (b) Transmission electron micrograph of nano-YSZ coated Mg–Ca alloy.

Triple-layer coating demonstrated only the presence of C and O (Fig. 3d) as a result of the formation of a thick PCL layer, where the underlayers' elements were not detected.

The cross-section morphology, in Fig. 4a, shows a NiCrAlY bond-coat with thickness of approximately 60–70 μm forming on the surface of the magnesium alloy. Large amount of voids, globular porosities and micro-cracks can also be observed. However, YSZ coating demonstrated bimodal structure composed of columnar grains as a result of solidification of the melted part of the powder, nanosize particles remaining from the unmelted or semi-melted parts and some equiaxed grains (Fig. 4b). The lamellar structure also can be easily detected indicating that the YSZ was built up layer by layer of individual splats which had melted or became semi-molten during spraying [31,34]. Two layer structures can be obviously seen which contain the YSZ layer with thickness of 150–160 μm as overlayer and NiCrAlY with a thickness of around 60–70 μm as an underlayer. Fig. 4c shows that PCL coating forms thick layer (70–80 μm) that homogeneously covers the surface of NiCrAlY/YSZ layers. It can also be observed that the PCL layer has good bonding with the YSZ plasma layer. In addition, it can be also seen that porosity in the plasma coated sample is much larger than that in the PCL coating. The presence of these coarse pores in

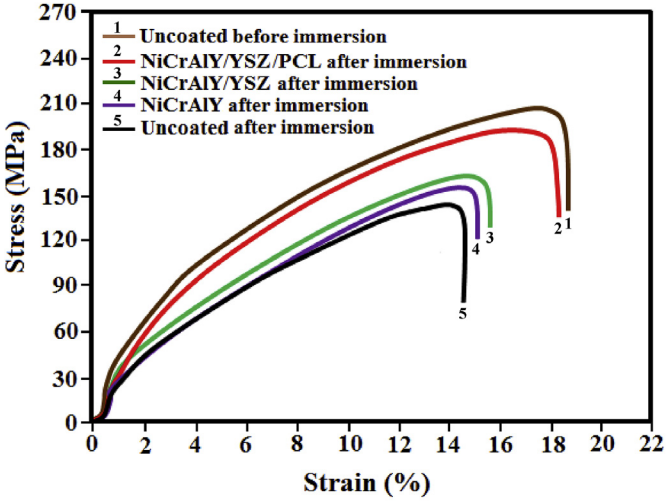

Fig. 6. Compressive stress–strain curves of uncoated, NiCrAlY, NiCrAlY/nano-YSZ, NiCrAlY/nano-YSZ/PCL coated Mg alloy before and after immersion in 3.5 wt.% NaCl solution for 10 days.

Table 2
Compression test results of the uncoated Mg–Ca alloy, single-layer NiCrAlY coated, dual-layer NiCrAlY/nano-YSZ coated and triple-layer NiCrAlY/nano-YSZ/PCL coated Mg alloy before and after immersion in 3.5 wt.% NaCl solution.

Specimen	Uncoated Mg alloy before immersion	Uncoated Mg alloy after 10 days immersion	NiCrAlY coated alloy after 10 days immersion	NiCrAlY/YSZ coated alloy after 10 days immersion	NiCrAlY/YSZ/PCL coated alloy after 10 days immersion
Compression strength –UCS (MPa)	212.4 ± 12	148.3 ± 7	157.2 ± 7	166.5 ± 8	197.3 ± 9

UCS: ultimate compressive strength.

plasma layers provides pathways for more infiltration of the aggressive corrosion solution through the coating during corrosion. Formation of a thick PCL coating over plasma layer leads to delay the contact between the corrosive species and Mg substrate.

The XRD patterns of the uncoated and coated samples are shown in Fig. 5a where the formation of the Mg_2Ca compound is seen in the uncoated samples. The NiCrAlY coating contain γ phase (Ni, Cr-rich), γ′ phase (Ni_3Al), $AlCr_3$ and some traces of β phase (AlNi) peaks. However, nanostructured YSZ include the tetragonal zirconia (t) only which can be attributed to rapid solidification during the process of APS. The triple-layer NiCrAlY/YSZ/PCL coating consists of two intense peaks at $2\theta = 21.6^\circ$ and $2\theta = 23.8^\circ$, that account for diffraction of the (110) and (200) planes, respectively. PCL has a crystalline structure with polyethylene-like orthorhombic cell disposition, with lattice parameters a = 0.748 nm, b = 0.498 nm, and c = 1.727 nm [35]. The TEM image in Fig. 5b shows that, after coating YSZ over NiCrAlY, equiaxed grains with a size distribution from several tens to several hundred nanometres formed. The orientation and size of these crystals strongly depend on the thermal conditions during spreading of molten droplets [36].

3.2. Mechanical properties

The compressive strength of uncoated, plasma coated, and plasma/polymer coated samples before and after immersion in 3.5 wt.% NaCl solution for 10 days are shown in Fig. 6. As the plasma and plasma/polymer coating did not affect the bulk mechanical properties, the compressive curves of uncoated and coated samples were similar before immersion. The compressive strengths of single-layer (NiCrAlY), dual-layer (NiCrAlY/nano-YSZ) and triple-layer (NiCrAlY/nano-YSZ/PCL) coated samples decreased from 212.4 MPa before immersion to 157.2, 166.5 and 197.3 MPa, respectively after 10 days of immersion in the NaCl solution (Table 2). However, the compressive curves of uncoated Mg–Ca dropped to 148.3 MPa after 10 days immersion because of the presence of pits and cracks caused by high corrosion rate. This indicates that plasma/polymer coating can effectively delay the loss of the mechanical properties of the substrate. High compressive strengths of the triple-layer coating after immersion, is because the polymer coating can prevent the direct contact between the Mg matrix and corrosive species. Thus, it acts as a barrier preventing the formation of galvanic cells at the interface between Mg/NiCrAlY bond-coating. The lower compressive strengths of single and dual-layer coatings are because the porous structure could not protect against corrosion. Microhardness of uncoated alloy was 49.2 Hv and this value significantly increased to 210.4 and 760.8 Hv after NiCrAlY and NiCrAlY/nano-YSZ plasma spray coating, as can be seen in Fig. 7a. This indicates that the dual-layer coating is approximately 12 times harder than that of the uncoated alloy. This can be due to the presence of semi-molten nanostructured particles in the YSZ structure, which act as crack arresters and enhanced splat-to-splat strength thereby, increasing coating toughness [15].

Fig. 7b shows that the bonding strength of the dual-layer NiCrAlY/nano-YSZ coating is about 14.5 MPa which is slightly higher than that of single-layer NiCrAlY coated Mg alloy (12.4 MPa). The most important mechanism of sprayed coatings adhesion is mechanical interlocking of the splats to the asperities of the substrate. The second mechanism is crack arresting by dense nanozones which embedded in the whole of microstructure. These mechanisms obviously describe the higher bonding strength of plasma spray coated samples compared to the plasma/polymer coated sample [15,37]. Higher bonding strength of dual-layer coating can be due to hindering of crack propagation *via* the unmolten or semi-molten particles (nanozone) as shown in Fig. 2h. However, poor bonding strength (7.6 MPa) was found for the triple-layer coating between the polymer and the plasma layer. This poor bonding strength may be attributed to the molecular structure of the polymer. PCL has a low ratio of O, which resulted in less electrostatic interaction with the nano-YSZ surface. Degner et al. [38] showed that PCL coating has low adhesion to the substrate strength. But coating still can effectively prevent corrosion of magnesium alloys which is in fact dependent on the polymer film thickness rather than the bonding strength.

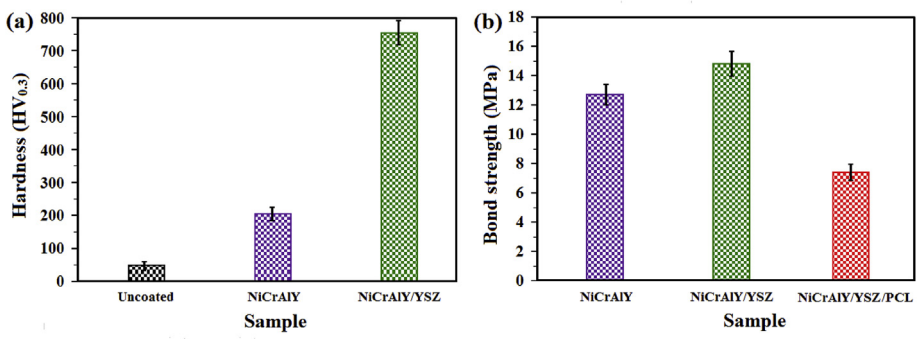

Fig. 7. (a) Hardness of uncoated, NiCrAlY and NiCrAlY/nano-YSZ coated Mg–Ca alloy and (b) Bond strengths of the NiCrAlY, NiCrAlY/nano-YSZ and NiCrAlY/nano-YSZ/PCL coated Mg–Ca alloy.

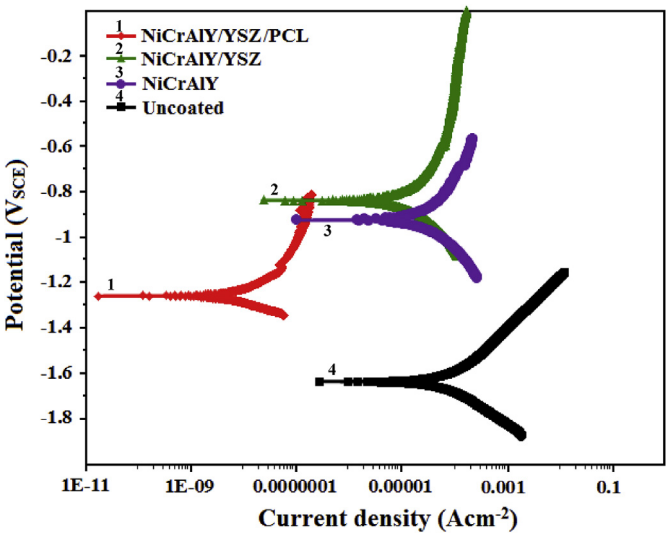

Fig. 8. Potentiodynamic polarization curves of uncoated, plasma coated and plasma/polymer coated Mg–Ca alloy specimens in 3.5 wt.% NaCl solution.

3.3. Electrochemical measurement

The electrochemical polarization curves of the uncoated Mg–Ca, single-layer NiCrAlY, dual-layer NiCrAlY/YSZ and triple-layer NiCrAlY/nano-YSZ/PCL coated samples in 3.5 wt.% NaCl solution are shown in Fig. 8. The corrosion potential (E_{corr}) showed that both plasma coatings and plasma/polymer coating significantly shifted the corrosion potential to more positive values. The E_{corr}, with reference to the uncoated magnesium alloy (−1631.4 mV_{SCE}), increased by −911.1 mV_{SCE} in single-layer coated samples. According to the mixed standard electrode potential theory [18,39], it was found that the air plasma spray coated samples were nobler than the uncoated Mg alloy. Electrochemical parameters of the uncoated and coated Mg samples in 3.5 wt% NaCL solution are listed in Table 3. The values of the corrosion current density (i_{corr}) of both single-layer (124.7 μA/cm^2) and dual-layer (89.3 μA/cm^2) samples were lower than that of the uncoated sample (285.3 μA/cm^2), while the triple-layer sample presented the lowest i_{corr} (0.14 μA/cm^2). The uncoated alloy presented higher i_{corr}, compared to the coated alloy, owing to the formation of a micro-galvanic cell between the Mg_2Ca phase and the α-Mg phase which resulted in an increase in the corrosion rate of the uncoated sample. On one hand, plasma spray coating can decrease i_{corr} of Mg alloy due to the protective nature of chromium and nickel, as well as the homogeneous coating composition. On other hand, due to the formation of galvanic corrosion cell between Mg substrate and metallic bond-coat (NiCrAlY) through porosities and micro-cracks which act as absorbent of corrosive solution, the plasma layer is not able to sufficiently protect the Mg substrate. However, triple-layer coating demonstrated the lowest i_{corr} because of the presence of the PCL coating as a top layer that sealed the porosity of the plasma coating and interrupted the penetration of the corrosive species. A corresponding increase in R_P from 1.21 kΩ cm^2 (for Mg–Ca) to 4.84, 5.62 and 687.8 kΩ cm^2 for single-layer, dual-layer and triple-layer coatings, respectively, was encountered. The large increase in R_p values observed for the triple-layer coating are due to the complete coverage of PCL on the plasma layer (NiCrAlY/YSZ) by a rather thicker triple-layer coating. The presence of pores and voids in plasma layer can provide the sites necessary to set up galvanic cells in corrosive solutions. Hydrogen gas produced by the cathodic reaction ruptures the coating [40]. However, PCL as top layer hinders the hydrogen evolution reaction increasing the corrosion resistance.

According to Eq. (2), the corrosion rate of triple-layer (0.003 mm/year) is significantly lower than that of dual-layer (2.04 mm/year), single-layer (2.84 mm/year) and uncoated (6.51 mm/year) samples. This obviously indicates the enhancement of protective properties of the specimens with triple-layer coating than that of the plasma coating and uncoated samples.

Nyquist plots of the uncoated, plasma coated and plasma/polymer coated samples acquired by electrochemical impedance spectra (EIS) are shown in Fig. 9a. In general, the high corrosion potential, charge transfer resistance and low corrosion current density indicate that the test specimen has good corrosion resistance [41]. As can be seen, coated and uncoated specimens showed a typical single-capacitive semi-circle, which represents the electrochemical process with only one time constant [42]. The capacitive loop in the high frequency region is related to the charge transfer reaction in the electric double-layer formed at the interface between the sample surface and corrosion medium [43]. The reason only one capacitive loop was observed in the Nyquist diagram is probably because the electrochemical reaction area at the metal/coating interface was still small in this immersion period. This led to the difficulty to separate the time relaxation of physical impedance of the coating from that of electrochemical reaction impedance at the metal/coating interface [43]. The equivalent circuit depicted in Fig. 9b was used to fit the impedance spectra in Fig. 9a whereby R_e represents the solution resistance, C_c is the coating capacitance, C_{dl} is the double layer capacitance and R_{ct} is the charge transfer resistance which is attributed to the electrochemical corrosion rate. The equivalent circuit in Model A is employed to characterize an uncoated sample while Model B could describe the coated samples. It can be clearly seen that sealing of plasma coating porosities by PCL leads to significant increase in the charge transfer resistance (R_t) of the triple-layer coated sample (2065.07 kΩ cm^2). This indicates that high level of corrosion protection of the Mg substrate can be obtained by polymer/plasma coating. However, the diameter of the semicircle in the Nyquist plots decreased to 2.21 and 2.52 kΩ cm^2 after single- and dual-layer plasma coating. This can be attributed to the ionic transport in the plasma coating including, e.g., chloride ion penetration through pores and the subsequent formation of a galvanic cell [44]. However, the lowest charge transfer resistance is observed for the uncoated sample (1.48 kΩ cm^2). The rate of the electrochemical processes at the substrate/electrolyte interface is controlled by the

Table 3
Electrochemical parameters of uncoated Mg–Ca alloy, single-layer NiCrAlY, dual-layer NiCrAlY/nano-YSZ and triple-layer NiCrAlY/nano-YSZ/PCL coated Mg alloy in 3.5 wt.% NaCl solution obtained from the polarization test.

Alloy	Corrosion potential, E_{corr} (mV vs. SCE)	Current density, i_{corr} (μA/cm^2)	Cathodic slope, $-\beta_C$ (mV/decade) vs. SCE	Anodic slope, β_a (mV/decade) vs. SCE	Polarization resistance, R_P (kΩcm^2)	Corrosion rate, P_i (mm/year)
Mg alloy	−1631.4 ± 13	285.3 ± 9	108 ± 6	125 ± 6	1.21 ± 0.2	6.51 ± 0.7
NiCrAlY coated	−911.1 ± 9	124.7 ± 5	141 ± 7	128 ± 6	4.84 ± 0.4	2.84 ± 0.3
NiCrAlY/nano-YSZ coated	−821.4 ± 8	89.3 ± 4	149 ± 6	132 ± 7	5.62 ± 0.7	2.04 ± 0.3
NiCrAlY/nano-YSZ/PCL coated	−1252.8 ± 11	0.14 ± 0.04	92 ± 5	65 ± 3	687.83 ± 17	0.003 ± 0.001

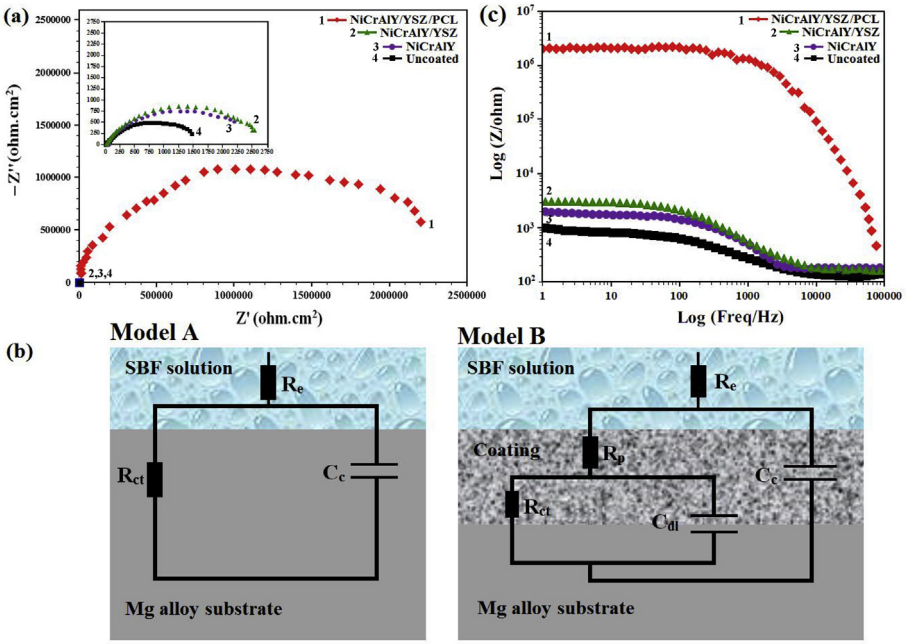

Fig. 9. (a) Nyquist plot, (b) Equivalent electrical circuit for uncoated (Model A) and coated samples (Model B), (c) Bode plot for the uncoated, plasma coated and plasma/polymer coated Mg alloy specimens in 3.5 wt.% NaCl solution.

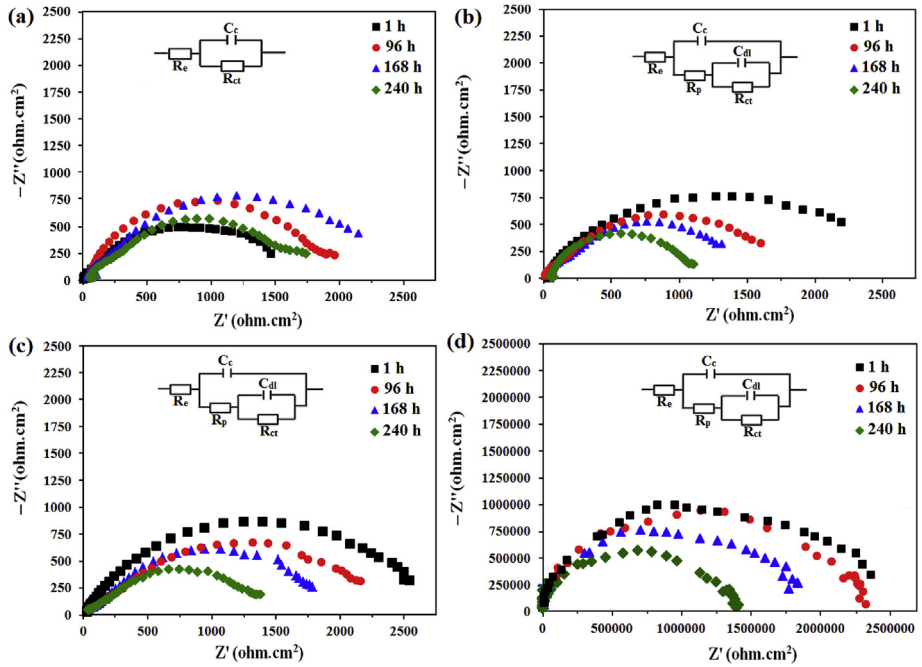

Fig. 10. Nyquist plots of, (a) uncoated, (b) NiCrAlY coated and (c) NiCrAlY/nano-YSZ coated and (d) NiCrAlY/nano-YSZ/PCL coated Mg alloy specimens in 3.5 wt.% NaCl solution at different immersion times.

charge-transfer resistance which is a key factor in determining the corrosion resistance [44,45]. This suggests that the triple-layer coating can significantly hinder the charge-transfer process at the sample/electrolyte interface.

The Bode plots of the EIS spectra obtained for both uncoated and coated samples are shown in Fig. 9c. The impedance modulus at low frequency (|Z|) is used to characterize the corrosion protection property of the coatings [44,45]. It is clear from the impedance value in the low frequency range that the triple-layer coatings presented the best corrosion protective behaviour as their |Z| value is the highest at the low frequency limit. Lower |Z| values of the other coatings which is attributed to the corrosion susceptibility of these samples. Polymer coating reduced porosity of plasma coating and improved barrier performance for corrosion protection. Moreover, the dependence of the corrosion resistance on the thickness of the coating suggests that the corrosion rate of triple-layer coated Mg can be adjusted by controlling its thickness [38]. This is because the formation of a thick PCL top layer postponed the

reach of the aggressive solution to the interface between NiCrAlY layer and Mg alloy substrate. The combination of polarization and impedance tests show that the triple-layer (NiCrAlY/YSZ/PCL) coating can efficiently delay the penetration of electrolyte through the coating, and thus enhance the corrosion barrier property.

In order to easily explore the protective ability of the plasma coated and plasma/polymer coated Mg samples, electrochemical impedance spectroscopy as a function of exposure time were measured (Fig. 10). It is obvious that in the initial stages the uncoated sample indicated lower impedance value. However, the impedance value increased as the immersion time was prolonged due to formation of corrosion products on the alloy surface which act as barrier layer. It is worth noting that the effect of barrier layer on impedance value decreased after 168 h exposure to the corrosive solution containing Cl^- due to the damage of the barrier film (Fig. 10a). The EIS spectra of uncoated sample can be fitted well using a simple equivalent circuit which is composed of C_c in parallel to the R_{ct} to represents interface between electrolyte and Mg alloy. EIS spectra from plasma coated and plasma/polymer coated Mg samples can be fitted by using a four-component model R(Q(R(QR))). From Nyquist plots of single-layer NiCrAlY coating sample a descending trend was found by escalating the immersion time indicating that the best barrier action of the plasma coating was found at short immersion time (Fig. 10b). This can be due to penetrating corrosive materials toward the substrate through the defects, porosities and voids which act as channels for formation of galvanic cells at the interface of coating/substrate. The spectra of bi-layer NiCrAlY/nano-YSZ coating presented similar features as the single-layer NiCrAlY coating (Fig. 10c). However, the Nyquist plots of triple-layer NiCrAlY/YSZ/PCL coated sample presented significantly larger semicircle during the entire exposure period, indicating a capacitive behaviour and barrier type protection polymer coating over plasma layers (Fig. 10d). The diameter of the semicircle in the Nyquist plots decreased gradually with exposure time, indicating that the triple-layer coating can efficiently delay infiltration of corrosive solution and chloride ions. However, after prolonged immersion time, coating was detached from the substrate and lost its protective property.

3.4. Immersion test

Fig. 11 shows the surface morphology of the uncoated, plasma coated, and plasma/polymer coated Mg samples immersed for 240 h in 3.5 wt.% NaCl solution. Uncoated Mg–Ca alloy presented extensive surface cracking that was accompanied by pitting corrosion (Fig. 11a,b). The crack formation is due to dehydration of

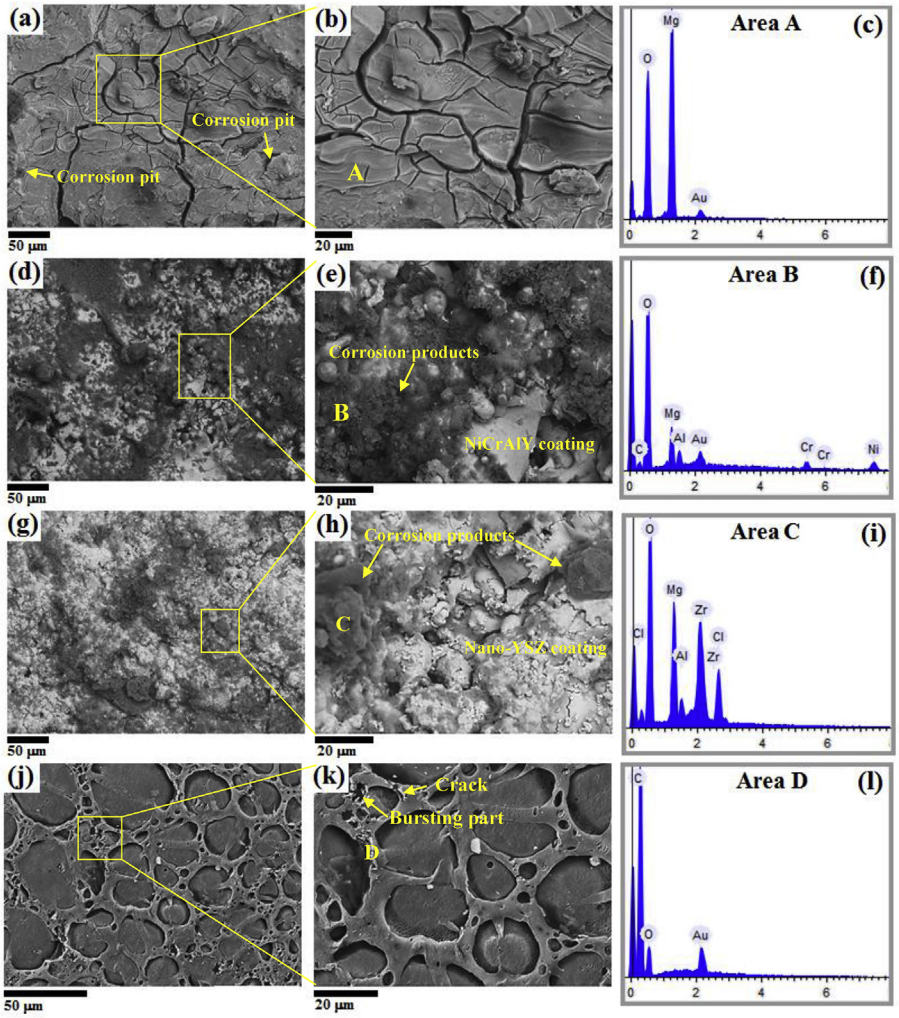

Fig. 11. FESEM micrographs of (a,b) uncoated Mg–Ca alloy, (d,e) NiCrAlY coating, (g,h) NiCrAlY/nano-YSZ coating and (j,k) NiCrAlY/nano-YSZ/PCL coated Mg alloy after immersion in 3.5% NaCl solution for 240 h and EDS analysis of (c) area A, (f) area B (i) area C and (l) area D.

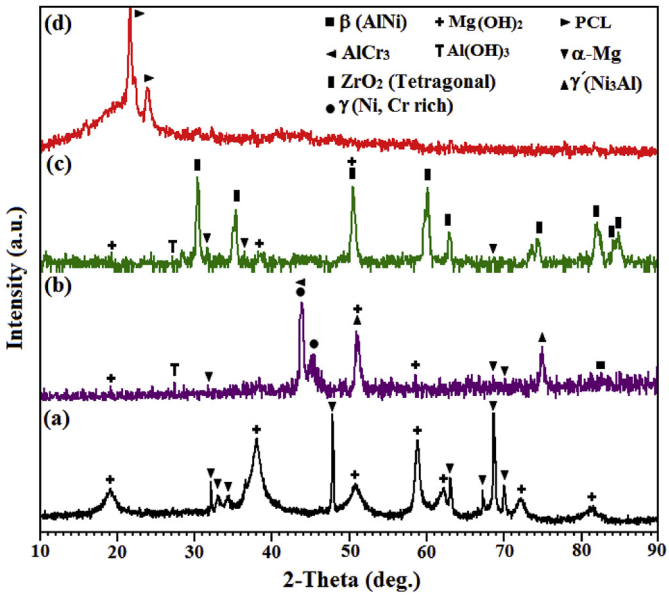

Fig. 12. X-ray diffraction patterns obtained from the corrosion products of (a) uncoated alloy, b) single-layer NiCrAlY coated Mg alloy, (c) dual-layer NiCrAlY/nano-YSZ coated Mg alloy and (d) triple-layer NiCrAlY/nano-YSZ/PCL coated specimens after full immersion in 3.5 wt.% NaCl solution for 240 h.

the corrosion products and associated differential shrinkage. Cracks make the solution contact the matrix easier, accelerating the corrosion of the matrix. EDS analysis in Fig. 11c shows the presence of Mg and O indicating that corrosion products are composed of magnesium hydroxide $Mg(OH)_2$ and the mole ratio of O to Mg was about 2.07. The XRD pattern in Fig. 12a further confirms the presence of $Mg(OH)_2$ (JCPDS file no. 44-1482) as the main corrosion product of the uncoated Mg–Ca. The Pilling Bedworth ratio (PBR) corresponding to MgO (magnesium oxide) is 0.81, while the reported PBR value for $Mg(OH)_2$ is about 1.77 [46]. A PBR value of less than unity indicates that the oxide formation would lead to volume shrinkage and tensile stress at the oxide/metal interface, which would imply poor protection against corrosion of the underlying metal [46]. The presence of $Mg(OH)_2$ can be found in conditions of pitting corrosion, without much access of air from the outside atmosphere, i.e. crevice corrosion [46]. Form Fig. 11d,e, it can be seen that large amount of corrosion products still accumulated on the surface of both single-layer NiCrAlY and dual-layer NiCrAlY/nano-YSZ coating. However, lower amount of corrosion products were observed in dual-layer than single-layer coating (Fig. 11g,h). The EDS analysis of the corrosion products of the single-layer coating revealed the presence of Mg, Al, and O indicating formation of $Mg(OH)_2$ and $Al(OH)_3$. Ni and Cr peaks seen in Fig. 11f are from the NiCrAlY layer. Single-layer coating acts as a semi-mechanical barrier consisted of a large number of voids and micro-cracks. Therefore, it could not adequately prevent the transfer of the metallic ions from the substrate. The EDS analysis of the dual-layer coating also shows the presence of Mg indicating that the corrosive solution can easily penetrate into the coating and corrode the substrate. Thus dual-layer plasma spray coating also could not effectively protect the substrate. The XRD analysis showed that the corrosion products in NiCrAlY and nano-YSZ coatings were mainly composed of $Mg(OH)_2$ and $Al(OH)_3$ (Fig. 12b,c). A small difference in the surface microstructure of triple-layer NiCrAlY/nano-YSZ/PCL coated sample was observed after immersion. Only small cracks are observed in the structure of triple-layer coating (Fig. 11j,k). Moreover, some parts had appeared to burst apart which may have been due to a build-up in pressure beneath the coating due to the evolution of H_2. The EDS analysis of triple-layer coating shown in Fig. 11l revealed the presence of C and O indicating that the structure of PCL remained unchanged proving that the PCL polymer coating over plasma-layers has great corrosion resistance in 3.5 wt% NaCl solution. XRD spectrum of the triple-layer coating indicates that the surface is composed of pure PCL (Fig. 12d). No corrosion product was found indicating that the surface of triple-layer NiCrAlY/nano-YSZ/PCL coating was intact and clean after 10 days immersion in 3.5 wt% NaCl solution. This once again shows that triple-layer coating significantly increases corrosion resistance of Mg alloy.

The EDS elemental mapping of corrosion products of uncoated and coated samples after immersion for 10 days is shown in Fig. 13. It can be seen that severe localized corrosion was found on the surface of the uncoated alloy. The corrosion products composed of Mg and O which covered the entire surface. The main constituents of the corrosion products of NiCrAlY coating is magnesium, oxygen and aluminium indicating formation of $Mg(OH)_2$ and $Al(OH)_3$ at the center and edge parts of the coating (Fig. 13b). However, most parts of NiCrAlY/nano-YSZ coating had mainly the elements present in the YSZ coating after 10 days of immersion, and the corrosion products were formed at the center part where the most aggressive attack took place (Fig. 13c). Polymer layer coating over plasma layer, maintained its original structure where no corrosion product could be detected on the PCL surface (Fig. 13d).

Fig. 14 shows a schematic illustration of the corrosion mechanism of uncoated, plasma coated and plasma/polymer coated samples in 3.5 wt% NaCl solution. When uncoated specimens are immersed in the NaCl solution, galvanic reactions between α-Mg and the Mg_2Ca phases occurred (Fig. 14a). As a result of this galvanic cell, the anodic and cathodic reactions occurred according to the following equations [47,48]:

$$Mg \rightarrow Mg^{+2} + 2e^{-} \text{ (Anodic reaction)} \quad (3)$$

$$2H_2O + 2e^{-} \rightarrow H_2 + 2OH^{-} \text{ (Cathodic reaction)} \quad (4)$$

The metal Mg transformed into insoluble $Mg(OH)_2$ film due to the reaction with OH^- and therefore magnesium hydroxide (brucite) as corrosion product started forming which resulted in decreasing corrosion rate of the specimens. This stage is also accompanied with strong hydrogen evolution. However, the presence of aggressive chloride ions in NaCl solution can destroy the protective layer by transforming the $Mg(OH)_2$ into more soluble $MgCl_2$ [49] according to the following reactions.

$$Mg + 2H_2O \rightarrow Mg(OH)_2\downarrow + H_2\uparrow \quad (5)$$

$$Mg(OH)_2\downarrow + 2Cl^{-} \rightarrow MgCl_2 + 2OH \quad -(6)$$

Breakdown of $Mg(OH)_2$ significantly decreases the protected area, subsequently increasing corrosion rate of the substrate. However, after NiCrAlY coating, further protection of the substrate was provided which resulted in reduction of corrosion attacks. However due to the presence of pores in the structure of plasma layer, the aqueous solution could easily diffuse through these defects and thus set up a galvanic cell at the interface of substrate/NiCrAlY layer (Fig. 14b). In this galvanic cell, the Mg alloy is anodic and the NiCrAlY is cathodic, hence Mg alloy corrodes significantly. With further infiltration of solution into the plasma layer, more corrosion occurs which leads to more corrosion products forming at the interface of plasma/substrate which destroyed the adhesion of the plasma layer to the substrate and debonded the coating subsequently losing the protection effect of the coating [50,51]. Dual-

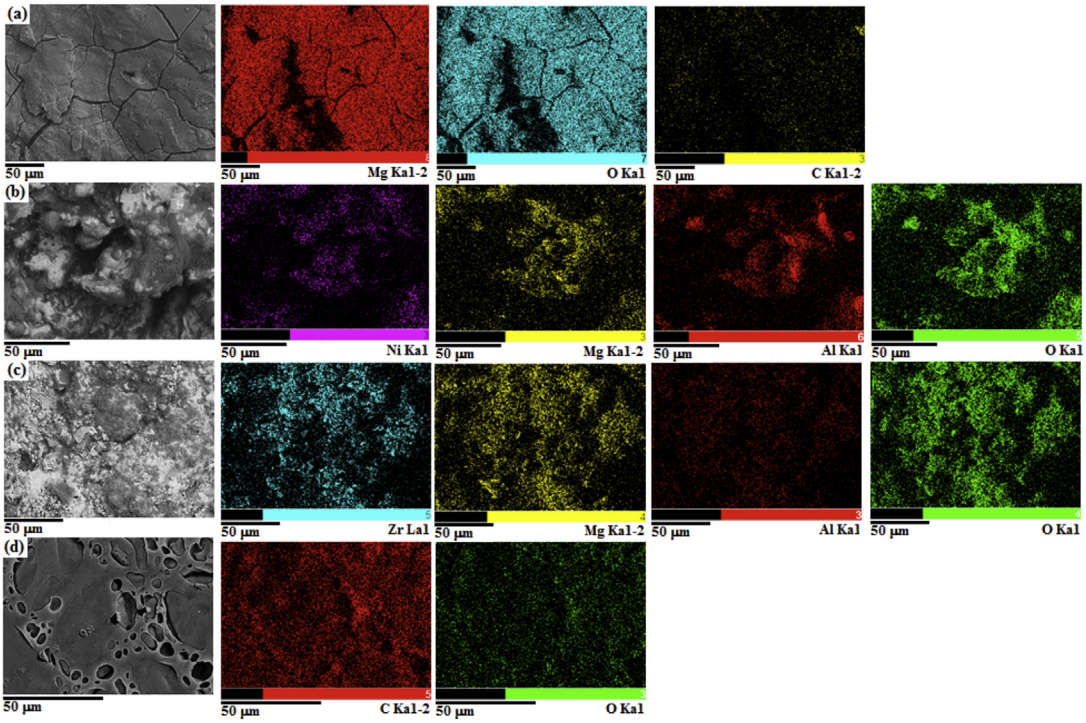

Fig. 13. Scanning electron micrographs and elemental mapping of (a) uncoated Mg alloy, (b) NiCrAlY coating, (c) NiCrAlY/nano-YSZ coating and (d) NiCrAlY/nano-YSZ/PCL coated Mg alloy after immersion in 3.5 wt.% NaCl solution for 240 h.

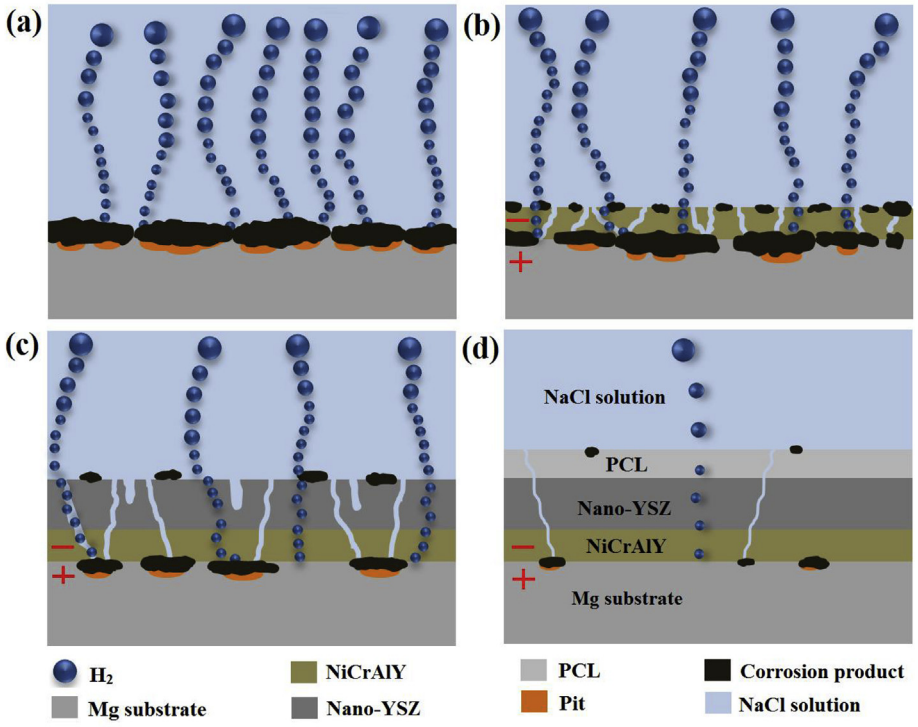

Fig. 14. Schematic illustration of the corrosion mechanism of (a) uncoated Mg–Ca alloy, (b) single-layer NiCrAlY, (c) dual-layer NiCrAlY/nano-YSZ and (d) triple-layer NiCrAlY/nano-YSZ/PCL coated Mg alloy after immersion in 3.5 wt% NaCl solution for 240 h.

layer NiCrAlY/nano-YSZ coating can provide more protection, but this layer is also porous, and the corrosive solution can still reach to the NiCrAlY layer through the micro-pores and micro-flaws of the overlayer (nano-YSZ). As soon as the solution reaches to the NiCrAlY layer, a strong galvanic cell occurs between the substrate and the plasma layer due to the large difference in corrosion potential (Fig. 14c). Therefore, it is necessary to improve the corrosion resistance of dual-layer coating to meet the different application

requirements. To address this issue, the plasma surface was coated with polymer (PCL) as an overlayer. After polymer coating, the surface of plasma layer is fully covered, thus transportation of corrosive ions (Cl^-) and electrolyte was largely blocked (Fig. 14d). Therefore, it can be stated that strong protective barrier was obtained by triple coating (NiCrAlY/nano-YSZ/PCL). However, upon increasing the immersion time, it is expected that more hydrogen gas would be released by the cathodic reaction that may cause bursting or delamination of the polymer film.

4. Conclusion

A novel method for the formation of a triple-layer NiCrAlY/nano-YSZ/PCL coating at the surface of Mg–Ca alloy has been established in this study. The underlayer is a porous and well adhered plasma coat (NiCrAlY/nano-YSZ), while the overlayer is a smooth and uniform hydrophobic polymer coat (PCL) which bonded to the pores of the plasma coat. Comparing with the uncoated and plasma coated Mg–Ca alloy, the plasma/polymer coated samples displayed much higher compressive strength after immersion in 3.5 wt% NaCl solution. However, the plasma coated samples indicted better bonding strength than plasma/polymer coated samples. The triple-layer plasma/polymer coating exhibited significantly lower corrosion current density (0.003 $\mu A/cm^2$) and higher R_p (687.83 $k\Omega cm^2$) than that of only single- or dual-layer plasma coated Mg–Ca samples. This is attributed to the sealing effect of the nano-YSZ plasma layer by the PCL polymer coating which considerably improved the corrosion protection of the Mg–Ca alloy. The immersion test displayed that the surface of triple-layer NiCrAlY/nano-YSZ/PCL coating was intact and clean after 10 days immersion in NaCl indicating that PCL polymer coating over plasma layer can provide long-term corrosion protection of a Mg–Ca alloy.

Acknowledgements

The authors would like to acknowledge the Universiti Teknologi Malaysia (UTM) and Nippon Sheet Glass Foundation for providing research facilities and financial support under Grant No. R.J.130000.7324.4B136.

References

[1] X.-J. Cui, X.-Z. Lin, C.-h. Liu, R.-S. Yang, X.-W. Zheng, M. Gong, Fabrication and corrosion resistance of a hydrophobic micro-arc oxidation coating on AZ31 Mg alloy, Corros. Sci. 90 (2015) 402–412.
[2] Z. Yao, Q. Xia, L. Chang, C. Li, Z. Jiang, Structure and properties of compound coatings on Mg alloys by micro-arc oxidation/hydrothermal treatment, J. Alloys Compd. 633 (2015) 435–442.
[3] Z. Song, Z. Xie, G. Yu, B. Hu, X. He, X. Zhang, A novel palladium-free surface activation process for electroless nickel deposition on micro-arc oxidation film of AZ91D Mg alloy, J. Alloys Compd. 623 (2015) 274–281.
[4] A. Zakiyuddin, K. Lee, Effect of a small addition of zinc and manganese to Mg–Ca based alloys on degradation behavior in physiological media, J. Alloys Compd. 629 (2015) 274–283.
[5] Y. Wan, G. Xiong, H. Luo, F. He, Y. Huang, X. Zhou, Preparation and characterization of a new biomedical magnesium–calcium alloy, Mater. Des. 29 (2008) 2034–2037.
[6] P. Sun, Y. Lu, Y. Yuan, X. Jing, M. Zhang, Preparation and characterization of duplex PEO/MoC coatings on Mg–Li alloy, Surf. Coat. Technol. 205 (2011) 4500–4506.
[7] Y. Xiong, C. Lu, C. Wang, R. Song, Degradation behavior of n-MAO/EPD bioceramic composite coatings on magnesium alloy in simulated body fluid, J. Alloys Compd. 625 (2015) 258–265.
[8] C. Wang, B. Jiang, M. Liu, Y. Ge, Corrosion characterization of micro-arc oxidization composite electrophoretic coating on AZ31B magnesium alloy, J. Alloys Compd. 621 (2015) 53–61.
[9] D.K. Ivanou, M. Starykevich, A.D. Lisenkov, M.L. Zheludkevich, H.B. Xue, S.V. Lamaka, M.G.S. Ferreira, Plasma anodized ZE41 magnesium alloy sealed with hybrid epoxy-silane coating, Corros. Sci. 73 (2013) 300–308.
[10] X. Ma, S. Zhu, L. Wang, C. Ji, C. Ren, S. Guan, Synthesis and properties of a bio-composite coating formed on magnesium alloy by one-step method of micro-arc oxidation, J. Alloys Compd. 590 (2014) 247–253.
[11] S.V. Gnedenkov, S.L. Sinebryukhov, D.V. Mashtalyar, V.S. Egorkin, M.V. Sidorova, A.S. Gnedenkov, Composite polymer-containing protective coatings on magnesium alloy MA8, Corros. Sci. 85 (2014) 52–59.
[12] X. Fan, Y. Liu, Z. Xu, Y. Wang, B. Zou, L. Gu, C. Wang, X. Chen, Z. Khan, D. Yang, X. Cao, Preparation and characterization of 8YSZ thermal barrier coatings on rare earth-magnesium alloy, J. Therm. Spray. Technol. 20 (2011) 948–957.
[13] H. Jamali, R. Mozafarinia, R. Shoja-Razavi, R. Ahmadi-Pidani, Comparison of hot corrosion behaviors of plasma-sprayed nanostructured and conventional YSZ thermal barrier coatings exposure to molten vanadium pentoxide and sodium sulfate, J. Eur. Ceram. Soc. 34 (2014) 485–492.
[14] M. Daroonparvar, M.A.M. Yajid, N.M. Yusof, H.R. Bakhsheshi-Rad, Fabrication and properties of triplex NiCrAlY/nano-Al_2O_3·13%TiO_2/nano-TiO_2 coatings on a magnesium alloy by atmospheric plasma spraying method, J. Alloys Compd. 645 (2015) 450–466.
[15] R.S. Lima, B.R. Marple, Thermal spray coatings engineered from nanostructured ceramic agglomerated powders for structural, thermal barrier and biomedical applications: a review, J. Therm. Spray. Technol. 16 (2007) 40–63.
[16] D. Wang, Z. Tian, L. Shen, Z. Liu, Y. Huang, Microstructural characteristics and formation mechanism of Al_2O_3–13 wt.% TiO_2 coatings plasma-sprayed with nanostructured agglomerated powders, Surf. Coat. Technol. 203 (2009) 1298–1303.
[17] X. Fan, J. Xu, Y. Wang, H. Ma, S. Zhao, X. Zhou, X. Cao, Preparation and corrosion resistance of MAO layer/Yb_2SiO_5 composite coating on Mg alloy, Surf. Coat. Technol. 240 (2014) 118–127.
[18] X. Fan, B. Zou, L. Gu, C. Wang, Y. Wang, W. Huang, L. Zhu, X. Cao, Investigation of the bond coats for thermal barrier coatings on Mg alloy, Appl. Surf. Sci. 265 (2013) 264–273.
[19] M. Mohedano, C. Blawert, M.L. Zheludkevich, Cerium-based sealing of PEO coated AM50 magnesium alloy, Surf. Coat. Technol. 269 (2015) 145–154.
[20] E.-J. Lee, S.-H. Teng, T.-S. Jang, P. Wang, S.-W. Yook, H.-E. Kim, Y.-H. Koh, Nanostructured poly(ε-caprolactone)–silica xerogel fibrous membrane for guided bone regeneration, Acta Biomater. 6 (2010) 3557–3565.
[21] H.M. Wong, K.W.K. Yeung, K.O. Lam, V. Tam, P.K. Chu, K.D.K. Luk, K.M.C. Cheung, A biodegradable polymer-based coating to control the performance of magnesium alloy orthopaedic implants, Biomaterials 31 (2010) 2084–2096.
[22] S.-I. Roohani-Esfahani, S. Nouri-Khorasani, Z. Lu, R. Appleyard, H. Zreiqat, The influence hydroxyapatite nanoparticle shape and size on the properties of biphasic calcium phosphate scaffolds coated with hydroxyapatite–PCL composites, Biomaterials 31 (2010) 5498–5509.
[23] G.R. Argade, K. Kandasamy, S.K. Panigrahi, R.S. Mishra, Corrosion behavior of a friction stir processed rare-earth added magnesium alloy, Corros. Sci. 58 (2012) 321–326.
[24] Z. Shi, M. Liu, A. Atrens, Measurement of the corrosion rate of magnesium alloys using Tafel extrapolation, Corros. Sci. 52 (2010) 579–588.
[25] M. Mezbahul-Islam, A.O. Mostafa, M. Medraj, Essential magnesium alloys binary phase diagrams and their thermochemical data, J. Mater 2014 (2014) 33.
[26] H.R. Bakhsheshi-Rad, M.H. Idris, M.R.A. Kadir, S. Farahany, Microstructure analysis and corrosion behavior of biodegradable Mg–Ca implant alloys, Mater. Des. 33 (2012) 88–97.
[27] H.Y. Tok, E. Hamzah, H.R. Bakhsheshi-Rad, The role of bismuth on the microstructure and corrosion behavior of ternary Mg–1.2Ca–xBi alloys for biomedical applications, J. Alloys Compd. 640 (2015) 335–346.
[28] M. Daroonparvar, M.A.M. Yajid, N.M. Yusof, H.R. Bakhsheshi-Rad, E. Hamzah, H.A. Kamali, Microstructural characterization and corrosion resistance evaluation of nanostructured Al and Al/AlCr coated Mg–Zn–Ce–La alloy, J. Alloys Compd. 615 (2014) 657–671.
[29] C. Lamuta, G. Di Girolamo, L. Pagnotta, Microstructural, mechanical and tribological properties of nanostructured YSZ coatings produced with different APS process parameters, Ceram. Int. 41 (2015) 8904–8914.
[30] R. Ghasemi, R. Shoja-Razavi, R. Mozafarinia, H. Jamali, M. Hajizadeh-Oghaz, R. Ahmadi-Pidani, The influence of laser treatment on hot corrosion behavior of plasma-sprayed nanostructured yttria stabilized zirconia thermal barrier coatings, J. Eur. Ceram. Soc. 34 (2014) 2013–2021.
[31] F. Tarasi, M. Medraj, A. Dolatabadi, J. Oberste-Berghaus, C. Moreau, Amorphous and crystalline phase formation during suspension plasma spraying of the alumina–zirconia composite, J. Eur. Ceram. Soc. 31 (2011) 2903–2913.
[32] Y. Wu, R.L. Clark, Controllable porous polymer particles generated by electrospraying, J. Colloid Interface Sci. 310 (2007) 529–535.
[33] P. Dayal, J. Liu, S. Kumar, T. Kyu, Experimental and theoretical investigations of porous structure formation in electrospun fibers, Macromol. 40 (2007) 7689–7694.
[34] F.H. Yuan, Z.X. Chen, Z.W. Huang, Z.G. Wang, S.J. Zhu, Oxidation behavior of thermal barrier coatings with HVOF and detonation-sprayed NiCrAlY bond-coats, Corros. Sci. 50 (2008) 1608–1617.
[35] M. Lebourg, J. Suay Antón, J.L. Gomez Ribelles, Characterization of calcium phosphate layers grown on polycaprolactone for tissue engineering purposes, Compos. Sci. Technol. 70 (2010) 1796–1804.
[36] X.-J. Ning, C.-X. Li, C.-J. Li, G.-J. Yang, Modification of microstructure and electrical conductivity of plasma-sprayed YSZ deposit through post-densification process, Mater. Sci. Eng. A 428 (2006) 98–105.
[37] C.R.C. Lima, J.M. Guilemany, Adhesion improvements of thermal barrier coatings with HVOF thermally sprayed bond coats, Surf. Coat. Technol. 201

(2007) 4694–4701.
[38] J. Degner, F. Singer, L. Cordero, A.R. Boccaccini, S. Virtanen, Electrochemical investigations of magnesium in DMEM with biodegradable polycaprolactone coating as corrosion barrier, Appl. Surf. Sci. 282 (2013) 264–270.
[39] G. Wu, A. Shanaghi, Y. Zhao, X. Zhang, R. Xu, Z. Wu, G. Li, P.K. Chu, The effect of interlayer on corrosion resistance of ceramic coating/Mg alloy substrate in simulated physiological environment, Surf. Coat. Technol. 206 (2012) 4892–4898.
[40] A. Srinivasan, P. Ranjani, N. Rajendran, Electrochemical polymerization of pyrrole over AZ31 Mg alloy for biomedical applications, Electrochim. Acta 88 (2013) 310–321.
[41] X. Ye, S. Cai, Y. Dou, G. Xu, K. Huang, M. Ren, X. Wang, Bioactive glass–ceramic coating for enhancing the in vitro corrosion resistance of biodegradable Mg alloy, Appl. Surf. Sci. 259 (2012) 799–805.
[42] C. Zhou, X. Lu, Z. Xin, J. Liu, Y. Zhang, Polybenzoxazine/SiO_2 nanocomposite coatings for corrosion protection of mild steel, Corros. Sci. 80 (2014) 269–275.
[43] X. Lu, Y. Zuo, X. Zhao, Y. Tang, X. Feng, The study of a Mg-rich epoxy primer for protection of AZ91D magnesium alloy, Corros. Sci. 53 (2011) 153–160.
[44] L. Chen, Y. Gu, L. Liu, S. Liu, B. Hou, Q. Liu, H. Ding, Effect of ultrasonic cold forging technology as the pretreatment on the corrosion resistance of MAO Ca/P coating on AZ31B Mg alloy, J. Alloys Compd. 635 (2015) 278–288.
[45] M. Liu, X. Mao, H. Zhu, A. Lin, D. Wang, Water and corrosion resistance of epoxy–acrylic–amine waterborne coatings: effects of resin molecular weight, polar group and hydrophobic segment, Corros. Sci. 75 (2013) 106–113.
[46] D. Sachdeva, Insights into microstructure based corrosion mechanism of high pressure die cast AM50 alloy, Corros. Sci. 60 (2012) 18–31.
[47] S. Sonmez, B. Aksakal, B. Dikici, Influence of hydroxyapatite coating thickness and powder particle size on corrosion performance of MA8M magnesium alloy, J. Alloys Compd. 596 (2014) 125–131.
[48] M. Ren, S. Cai, T. Liu, et al., Calcium phosphate glass/MgF_2 double layered composite coating for improving the corrosion resistance of magnesium alloy, J. Alloys Compd. 591 (2014) 34–40.
[49] Y. Chen, Y. Song, S. Zhang, J. Li, C. Zhao, X. Zhang, Interaction between a high purity magnesium surface and PCL and PLA coatings during dynamic degradation, Biomed. Mater 6 (2011) 1–8.
[50] H.R. Bakhsheshi-Rad, E. Hamzah, A.F. Ismail, M. Daroonparvar, M. Kasiri-Asgarani, S. Jabbarzare, M. Medraj, Microstructural, mechanical properties and corrosion behavior of plasma sprayed NiCrAlY/nano-YSZ duplex coating on Mg–1.2Ca–3Zn alloy, Ceram.Int. 41 (2015) 15272–15277.
[51] H.R. Bakhsheshi-Rad, E. Hamzah, M.R. Abdul-Kadir, M. Daroonparvar, M. Medraj, Corrosion and mechanical performance of double-layered nano-Al/PCL coating on Mg–Ca–Bi alloy, Vacuum 119 (2015) 95–98.